Toward efficacy of piecewise polynomial truncated singular value decomposition algorithm in moving force identification

Zhen Chen[a,b*], Lifeng Qin[a], Shunbo Zhao[a*], Tommy H.T. Chan[b], Andy Nguyen[c]

[a] *International Joint Research Lab for Eco-building Materials and Engineering of Henan, North China University of Water Resources and Electric Power, Zhengzhou 450045, China*
[b] *School of Civil Engineering and Built Environment, Queensland University of Technology (QUT), Brisbane, 4000, Australia*
[c] *School of Civil Engineering of Surveying, University of Southern Queensland (USQ), Springfield Central, 4300, Australia*

Abstract: This paper introduces and evaluates the piecewise polynomial truncated singular value decomposition (PP-TSVD) algorithm toward an effective use for moving force identification (MFI). Suffering from numerical non-uniqueness and noise disturbance, the MFI is known to be associated with ill-posedness. An important method for solving this problem is the truncated singular value decomposition (TSVD) algorithm but the truncated small singular values removed by TSVD may contain some useful information. The PP-TSVD algorithm extracts the useful responses from truncated small singular values and superposes it into the solution of TSVD, which can be useful in MFI. In this paper, a comprehensive numerical simulation is set up to evaluate PP-TSVD, and compare this technique against TSVD and SVD. Numerically simulated data are processed to validate the novel method, which show that regularization matrix **L** and truncating point k are two most important governing factors affecting identification accuracy and ill-posedness immunity of PP-TSVD.

Keywords: moving force identification, piecewise polynomial truncated singular value decomposition, ill-posedness, regularization matrix, truncating point

1 Introduction

The identification of moving forces acting on bridges is an important practical problem in structural dynamics, for instance, to guide the design of bridges as live load components in the bridge design code. Although the forward model of load identification has been established, most of the identification methods involve in singular value decomposition (SVD) in the identification process. In addition, the small singulars of the system matrix decide the great degree of system ill-posedness and lead to a large identified error (Liu et al., 2017). In the past, there has been significant research effort to solve this problem by Chan et al. (2001, 2006).

Comparative studies (Yu and Chan, 2007) show that the time domain method (TDM) (Law et al., 1997) and frequency-time domain method (FTDM) (Law et al., 1999) are clearly better than those from both interpretive method I (IMI) (O'Connor and Chan, 1998) and interpretive method II (IMII) (Chan et al., 1999). The inverse problems involving dynamic parameter identification in time domain or frequency-time domain have been studied by many researchers (Zhu and Law, 2006; Zhu et al., 2018). However, due to matrix ill-posedness and noise disturbance in moving force identification (MFI), the identification accuracy of many methods is still not high enough since the nature of the inverse problem is ill-posed (Yu et al., 2016).

The Tikhonov regularization approach is very effective with ill-posed problems due to matrix ill-posedness and noise disturbance (Busby and Trujillo, 1997). Choi et al. (2007) indicated that the reconstructed forces can be improved by choosing the optimal regularization parameter of Tikhonov regularization. Ding et al. (2015) presented unscented Kalman filter technique to identify the structural parameters and coefficients of the orthogonal decomposition. Ronasi et al. (2011) adopted the traditional Tikhonov regularization as a means to further reduce the impact of noise on choosing the suitable resolution for the sought load. Lu and Liu (2011) proposed a dynamic

*Corresponding author.
E-mail address: yuchenfish@163.com (Z. Chen), sbzhao@ncwu.edu.cn (S. Zhao).

response sensitivity-based finite element model updating approach to identify both the vehicular parameters and the structural damages. Li et al. (2013) presented an adaptive Tikhonov regularization technique to improve the damage identification results when noise effect is included. Liu et al. (2015) adopted an improved regularization to overcome the ill-posedness of load reconstruction by selecting the filter function. Besides Tikhonov regularization, there are many other optimization methods with properties that make them better suited to certain problems to combat the ill-posedness (Sanchez and Benaroya, 2014).

Recent years have witnessed many new approaches adopted for solving the MFI problem such as updated static component technique (Pinkaew, 2006), cross entropy optimization approach (Dowling et al., 2012), Bayesian inference regularization (Feng et al., 2015), truncated generalized singular value decomposition algorithm (Chen and Chan, 2017), modified preconditioned conjugate gradient method (Chen et al., 2018) and weighted l_1-norm regularization method (Pan et al., 2018). The SVD technique is much better than direct pseudo-inverse solution for MFI with TDM but the identification accuracy is still sensitive to perturbations. The truncated singular value decomposition (TSVD) technique has been widely used in discrete linear ill-posed problems, which provides significant improvements to the least-squares estimator to derive a single optimal solution for a given problem (Xu, 1998; Bouhamidi et al., 2011). The TSVD uses only the largest singular values to derive the solution and small singular values are more or less arbitrarily discarded. By truncating the small singular values, TSVD can effectively filter the noise component in measurement responses but the truncating process inevitably discards some true responses including in small singular values. Studies by Winkler (1997a, 1997b) indicated that an important aspect in using TSVD is the deletion of the correct number of singular values of the coefficient matrix and polynomial basis conversion can be used to improve this problem.

Hansen and Mosegaard (1996) presented a piecewise polynomial truncated singular value decomposition (PP-TSVD) approach but the choosing of the optimal parameter has not been proposed. The PP-TSVD algorithm extracts the true responses from truncated small singular values and superposes it into the solution of TSVD, which offset the disadvantage of TSVD perfectly. Giustolisi (2003) indicated that the PP-TSVD can overcome poor generalization properties due to the high dimensionality and non-Gaussian noise. Sobouti et al. (2016) adopted the PP-TSVD to solve the total variation regularized inverse problem. However, there has been a lack of study on evaluation of the PP-TSVD and absent rules for choosing the optimal parameter of the PP-TSVD.

As mentioned above, the PP-TSVD method is very effective in solving the linearized ill-posed problems, which has excellent theoretical completeness and offset the disadvantage of TSVD perfectly. In this paper, a comprehensive numerical simulation survey is set up to compare this algorithm against TSVD and SVD. Furthermore, the governing regularization parameters of the PP-TSVD have been scrutiny selected, such as the regularization matrix **L** and the truncating point k. The numerical results show that the PP-TSVD has significant improvement compared with TSVD and TDM, which has important theoretical and provide a useful approach for the MFI.

2 Theory of moving force identification

2.1. Theory of time domain method (TDM)

As shown in Fig. 1, assuming the bridge is of constant cross-section with constant mass per unit length ρ, having linear, viscous proportional damping C and with span length L, Young's modulus E and second moment of inertia of the beam cross-section I, neglecting the effects of shear deformation and rotary inertia, and with the force $f(t)$ moving from left to right at a prescribed velocity c at time t, the equation of motion in terms of the modal coordinate $q_n(t)$can be written as

$$\ddot{q}_n(t) + 2\xi_n\omega_n\dot{q}_n(t) + \omega_n^2 q_n(t) = \frac{2}{\rho L}p_n(t) \qquad (\mathrm{n} = 1,2,\dots,\infty) \tag{1}$$

where $p_n(t) = f(t)\sin\frac{n\pi ct}{L}$ is the modal force; $\omega_n = \frac{n^2\pi^2}{L^2}\sqrt{\frac{EI}{\rho}}$ is the n-th modal frequency; $\xi_n = \frac{C}{2\rho\omega_n}$ is the modal damping ratio.

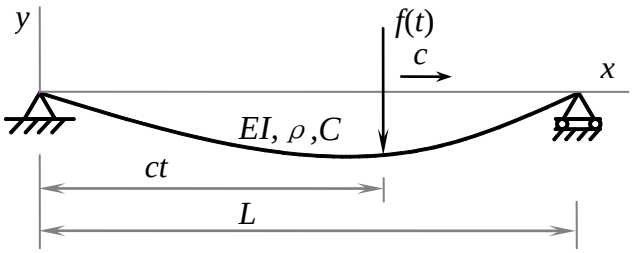

Fig. 1. Model of moving force identification

Equation (1) can be solved in the time domain by the convolution integral, yielding

$$q_n(t) = \frac{2}{\rho L}\int_0^t h_n(t-\tau)\,p(\tau)d\tau \tag{2}$$

where $h_n(t) = \frac{1}{\omega_n^{'}}e^{-\xi_n\omega_n t}\sin(\omega_n^{'}t)$ and $\omega_n' = \omega_n\sqrt{1-\xi_n^2}$.

At point x and time t, the deflection $\mathbf{v}(x,t)$ of the simply supported beam can be expressed as Law et al. (1997) with modal superposition

$$\mathbf{v}(x,t) = \sum_{n=1}^{\infty}\frac{2}{\rho L\omega_n'}\sin\frac{n\pi x}{L}\int_0^t e^{-\xi_n\omega_n(t-\tau)}\sin\omega_n'(t-\tau)\sin\frac{n\pi c\tau}{L}f(\tau)\mathrm{d}\tau \tag{3}$$

At point x and time t, the bending moment $\mathbf{M}(x,t)$ of the simply supported beam can be expressed as

$$\mathbf{M}(x,t) = -EI\frac{\partial^2 v(x,t)}{\partial x^2} = \sum_{n=1}^{\infty}\frac{2EI\pi^2}{\rho L^3}\frac{n^2}{\omega_n'}\sin\frac{n\pi x}{L}\int_0^t e^{-\xi_n\omega_n(t-\tau)}\sin\omega_n'(t-\tau)\sin\frac{n\pi c\tau}{L}f(\tau)\mathrm{d}\tau \tag{4}$$

Assuming that the time-varying force $f(t)$ is a step function about the time sampling interval Δt, and then the equation (4) can be rewritten in discrete terms as

$$M(i) = \frac{2EI\pi^2}{\rho L^3}\sum_{n=1}^{\infty}\frac{n^2}{\omega_n^{'}}sin\frac{n\pi x}{L}\sum_{j=0}^{i}e^{-\xi_n\omega_n\Delta t(i-j)}\,sin\,\omega_n^{'}\,\Delta t(i-j)\sin\frac{n\pi c\Delta tj}{L}f(j) \qquad i = (0,1,2,\dots,\mathrm{N}) \tag{5}$$

where $\mathrm{N}+1$ is the number of sample points. Let

$$C_{xn} = \frac{2EI\pi^2}{\rho L^3}\frac{n^2}{\omega_n^{'}}sin\frac{n\pi x}{L}\Delta t \qquad E_n^{i-j} = e^{-\xi_n\omega_n\Delta t(i-j)}$$
$$S_1(i-j) = sin\,\omega_n^{'}\,\Delta t(i-j) \qquad S_2(j) = sin(\frac{n\pi c\Delta t}{L}j) \tag{6}$$

Then the equation (5) can be arranged into matrix form as

$$\begin{Bmatrix}M(0)\\M(1)\\M(2)\\\vdots\\M(N)\end{Bmatrix} = \sum_{n=1}^{\infty}C_{nx}\times\begin{bmatrix}0 & 0 & 0 & \cdots & 0\\0 & 0 & 0 & \cdots & 0\\0 & E_n^1S_1(1)S_2(1) & 0 & \cdots & 0\\\vdots & \vdots & \vdots & \ddots & \vdots\\0 & E_n^{N-1}S_1(N-1)S_2(1) & E_n^{N-2}S_1(N-2)S_2(2) & \cdots & E_n^{N-N_B}S_1(N-N_B)S_2(N_B)\end{bmatrix}\times\begin{Bmatrix}f(0)\\f(1)\\f(2)\\\vdots\\f(N_B)\end{Bmatrix} \tag{7}$$

where $N_B = \frac{L}{c\Delta t}$. The time-varying force $f(t)$ is equal to 0 when the vehicle just get on or off the bridge, that is, $f(0) = 0$ and $f(N_B) = 0$ which corresponding to $M(0) = 0$ and $M(1) = 0$.

Then the equation (7) can be condensed as

$$\begin{Bmatrix}M(2)\\M(3)\\\vdots\\M(N)\end{Bmatrix} = \sum_{n=1}^{\infty}C_{nx}\times\begin{bmatrix}E_n^1S_1(1)S_2(1) & 0 & \cdots & 0\\E_n^1S_1(2)S_2(1) & E_n^1S_1(1)S_2(2) & \cdots & 0\\\vdots & \vdots & \ddots & 0\\E_n^{N-1}S_1(N-1)S_2(1) & E_n^{N-2}S_1(N-2)S_2(2) & \cdots & E_n^{N-N_B+1}S_1(N-N_B+1)S_2(N_B-1)\end{bmatrix}\times\begin{Bmatrix}f(1)\\f(2)\\\vdots\\f(N_B-1)\end{Bmatrix} \tag{8}$$

where $M(i)$ is the bending moment of the i-th sampling interval and $f(i)$ is the axle force of the i-th sampling interval.

Equation (8) is simply rewritten as

$$\underset{(N-1)(N_B-1)}{B} \cdot \underset{(N_B-1)\times 1}{f} = \underset{(N-1)\times 1}{M} \tag{9}$$

Similarly, at point x and time t, the acceleration $\ddot{\mathbf{v}}(x,t)$ of the simply supported beam can be expressed as

$$\ddot{\mathbf{v}}(x,t) = \sum_{n=1}^{\infty} \frac{2}{\rho L} \sin\frac{n\pi x}{L} \left[f(t)\sin\frac{n\pi x}{L} + \int_0^t \ddot{h}_t(t-\tau) f(\tau) \sin\frac{n\pi c\tau}{L} \mathrm{d}\tau \right] \tag{10}$$

where $\ddot{h}_n(t) = \frac{1}{\omega_n^{'}} e^{-\xi_n \omega_n t} \times \{[(\xi_n\omega_n)^2 - \omega_n^{'2}] \sin\omega_n^{'} t + (-2\xi_n\omega_n\omega_n^{'}) \cos\omega_n^{'} t\}$.

Equation (10) can also be arranged into matrix form and simply rewritten as

$$\underset{N\times 1}{\ddot{v}_n} = \underset{N\times(N_B-1)}{A_n} \cdot \underset{(N_B-1)\times 1}{f} \tag{11}$$

As shown above, the relationship between the time-varying force $f(t)$ and the bending moment responses or acceleration responses can be rewritten in discrete terms and rearranged into a set of linear equations, which also can be modified for the identification of multi-forces in terms of the linear superposition principle.

2.2 Theory of truncated singular value decomposition (TSVD)

The singular value decomposition of system matrix **A** in MFI can be described as

$$\mathbf{A} = \mathbf{U}\boldsymbol{\Sigma}\mathbf{V}^T = \sum_{i=1}^{n} \mathbf{u}_i \, \boldsymbol{\sigma}_i \mathbf{v}_i^T \tag{12}$$

where $\mathbf{U} = (\mathbf{u}_1, \mathbf{u}_2, \cdots \mathbf{u}_n)$ and $\mathbf{V} = (\mathbf{v}_1, \mathbf{v}_2, \cdots \mathbf{v}_n)$ are orthonormal columns matrices with $\mathbf{U}^T\mathbf{U} = \mathbf{V}^T\mathbf{V} = \mathbf{I}_n$, $\mathbf{u}_i\mathbf{u}_i^T = 1$, $\mathbf{v}_i\mathbf{v}_i^T = 1$, $\sum = \mathrm{diag}(\sigma_1, \sigma_2, \cdots, \sigma_n)$ with $\sigma_1 \geq \sigma_2 \geq \cdots \geq \sigma_n \geq 0$. The first singular values of vehicle-bridge system matrix **A** is σ_1 and the n-th singular values of matrix **A** is σ_n, then the condition number of system matrix **A** is $\frac{\sigma_1}{\sigma_n}$. With one or more very small singular values existing in system matrix, the condition number of system matrix **A** is very large relative to σ_1 and then leading to ill-posedness of MFI. The best approach to reduce the abnormal large condition number of **A** is to truncate very small singular values by using TSVD.

The TSVD approach can be described as

$$\mathbf{A}_k = \mathbf{U}\boldsymbol{\Sigma}\mathbf{V}^T = \sum_{i=1}^{k} \mathbf{u}_i \, \boldsymbol{\sigma}_i \mathbf{v}_i^T \qquad k \leq n \tag{13}$$

Then the solutions of vehicle-bridge system equation $\mathbf{Ax} = \mathbf{b}$ with TSVD approach can be described as the minimization problem

$$\min\|\mathbf{x}\|_2 \quad \text{subject to} \quad \min\|\mathbf{A}_k\mathbf{x} - \mathbf{b}\|_2 \tag{14}$$

The solution of TSVD can be obtained as

$$\mathbf{x}_k = {\mathbf{A}_k}^{-1}\mathbf{b} = \left(\sum_{i=1}^{k} \mathbf{u}_i \, \boldsymbol{\sigma}_i \mathbf{v}_i^T\right)^{-1}\mathbf{b} \qquad k \leq n \tag{15}$$

According to the property of vectors $\mathbf{u}_i$ and $\mathbf{v}_i$, the TSVD solutions of $\mathbf{Ax} = \mathbf{b}$ can be expressed as

$$\mathbf{x}_k = \sum_{i=1}^{k} \frac{\mathbf{u}_i^T\mathbf{b}}{\boldsymbol{\sigma}_i}\mathbf{v}_i \tag{16}$$

The 2-norm of $\mathbf{x}_k$ satisfies $\|\mathbf{x}_k\|_2^2 = \sum_{i=1}^{k} {\sigma_i}^{-2}\left(\mathbf{u}_i^T\mathbf{b}\right)^2$, and thus $\|\mathbf{x}\|_2$ is increased with k. The truncating point k is an important regularization parameter of the TSVD, which controls the amount of stabilization imposed on $\mathbf{x}_k$ and the ill-posedness immunity of TSVD. Although the TSVD is well known as a useful method for model regularization, it

still has some limitations such as the data over-fitting problem. Therefore, the PP-TSVD is presented to avoid data over-fitting problem since some additional responses are extracted from truncated small singular values compared with TSVD.

2.3 Theory of piecewise polynomial truncated singular value decomposition (PP-TSVD)

The regularization of $\|\mathbf{x}\|_2$ is often more appropriate by minimizing the seminorm $\|\mathbf{Lx}\|_2$. $\mathbf{L}$ is the regularization matrix which can be obtained from discrete approximation of derivative operators. Assuming that $\mathbf{L}$ is $\big(n-(p-1)\big)\times n$ and has full row rank, the $p-1$ is less than truncating point k corresponding to $(p-1)$-th derivative operator, in which the seminorm $\|\mathbf{Lx}\|_2$ is introduced to replace the original linear system $\min\|\mathbf{x}\|_2$, i.e.,

$$\min\|\mathbf{Lx}\|_2 \quad \text{subject to} \quad \min\|\mathbf{A}_k\mathbf{x}-\mathbf{b}\|_2 \tag{17}$$

By introducing the matrix $\mathbf{V}_k$ consisting of null vectors of $\mathbf{A}_k$ as

$$\mathbf{V}_k=(\mathbf{v}_{k+1},\mathbf{v}_{k+2},\cdots,\mathbf{v}_n) \tag{18}$$

In order to extract some additional responses from truncated small singular values of TSVD, the solution $\mathbf{x}_\mathrm{L}$ consists of the TSVD solution $\mathbf{x}_k$ plus a modification, which can be expressed as

$$\mathbf{x}_\mathrm{L}=\mathbf{x}_k-\mathbf{V}_k(\mathbf{LV}_k)^+\mathbf{Lx}_k \tag{19}$$

where $(\mathbf{LV}_k)^+$ is the pseudoinverse of $\mathbf{LV}_k$. Form a computational point of view, the vector $\mathbf{w}_k=(\mathbf{LV}_k)^+\mathbf{Lx}_k$ is simply the least squares solution to the problem $\min\|(\mathbf{LV}_k)\mathbf{w}_k-\mathbf{Lx}_k\|_2$.

The PP-TSVD algorithm is derived from equation (17) by replacing the 2-norm of $\mathbf{Lx}$ with the 1-norm. Thus, the solution of the above problem can be expressed as Hansen and Mosegaard (1996)

$$\min\|\mathbf{Lx}\|_1 \quad \text{subject to} \quad \min\|\mathbf{A}_k\mathbf{x}-\mathbf{b}\|_1 \tag{20}$$

Then the solution of PP-TSVD $\mathbf{x}_{\mathrm{L},k}$ can be expressed as

$$\mathbf{x}_{\mathrm{L},k}=\mathbf{x}_k-\mathbf{V}_k\mathbf{w}_k \tag{21}$$

Similarly, the vector $\mathbf{w}_k$ can be solved by the following linear l_1 problem

$$\min\|(\mathbf{LV}_k)\mathbf{w}_k-\mathbf{Lx}_k\|_1 \tag{22}$$

The basic procedure for MFI by using PP-TSVD algorithm is shown in Fig. 2. As shown in Fig. 2, there are two important regularization parameters, one is regularization matrix $\mathbf{L}$ and the other is truncating point k.

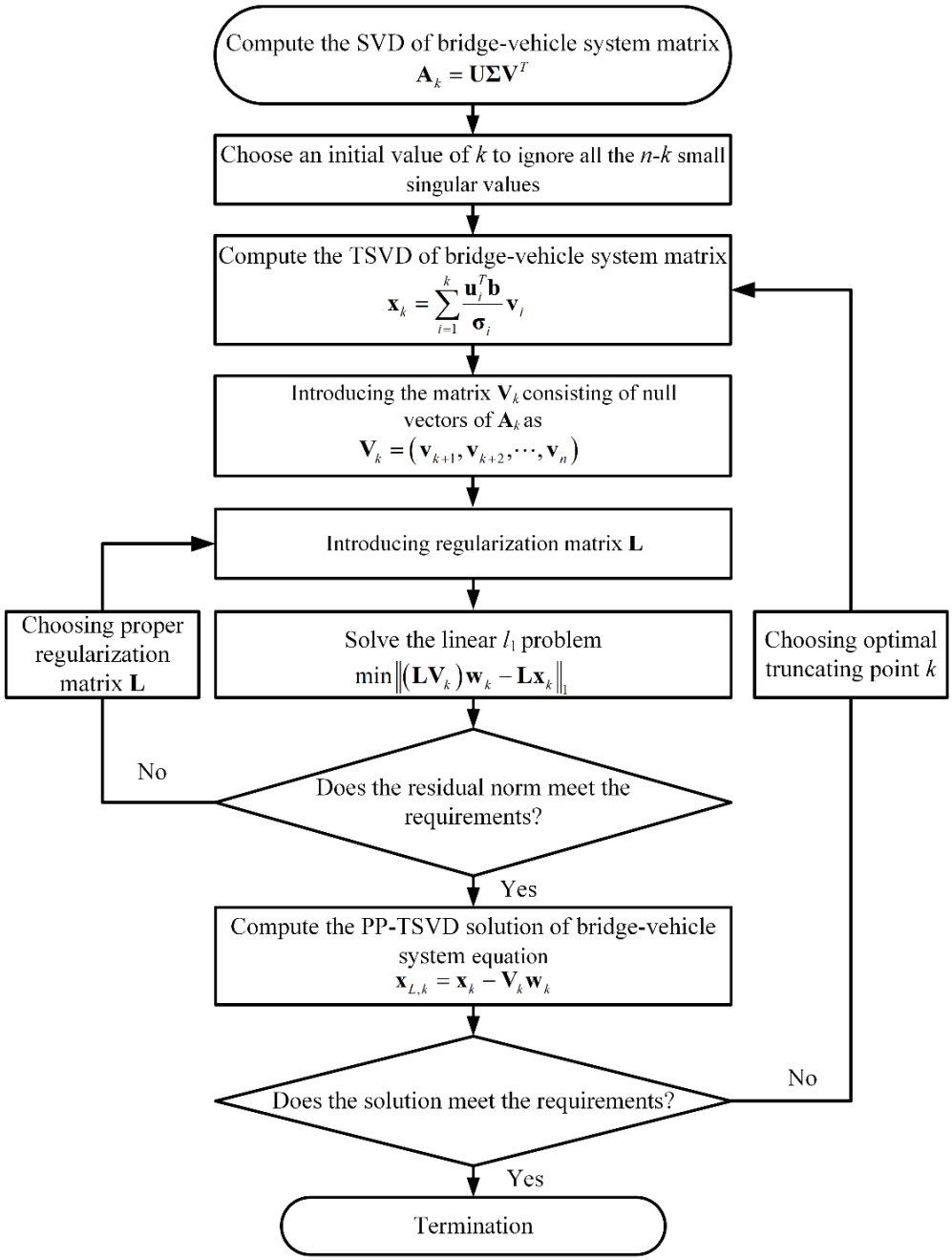

Fig. 2. Basic procedure for moving force identification by using PP-TSVD algorithm

3 Computational Verification and Validation

3.1 Simulation parameters of vehicle and bridge

There are 8 cases studied in this section as shown in 1st column in Table 1. Two kinds of measuring sensors are arranged on the 1/4, 1/2 and 3/4 span of the bridge, respectively. The first one is accelerometer which can be used to measure acceleration responses directly. The second one is strain gauge which can be used to measure bending moment responses indirectly. The relationship between bending moment responses and voltage signals of strain gauge can be calibrated by static step-by-step loading test of bridge or derived from the mechanical analysis.

The biaxial time-varying forces are expresses as follows

$$f_1(t) = 58\,800[1 + 0.1\sin(10\pi t)]\ \mathrm{N}$$
$$f_2(t) = 137\,200[1 + 0.1\sin(10\pi t)]\ \mathrm{N} \quad (23)$$

The parameters of the biaxial time-varying forces and the simply supported beam are extracted and modified from Yu et al. (2008). The rear axle load is heavier than the front axle load which is similar to the actual truck load. The parameters of the biaxial time-varying forces are as follows: the moving speed is $c = 40\mathrm{m\,s^{-1}}$ and the distance between two forces is 8 m. The parameters of the simply supported beam are as follows: $L = 40\mathrm{m}$, $EI = 1.27 \times$

10^{11} N m^2, $\rho A = 12\,000$kg m^{-1} and the first four natural frequencies of simply supported beam are 3.2Hz, 12.8Hz, 28.8Hz, and 51.2Hz, respectively. The analysis frequency of the numerical simulation is from 0Hz to 40Hz and the sampling frequency is 200Hz.

The measured responses are polluted with random noise, which can be expressed as

$$\mathbf{R}_{\text{measured}} = \mathbf{R}_{\text{calculated}} \cdot (1 + E_p \cdot \mathbf{N}_{\text{noise}}) \tag{24}$$

where E_p represents white error level choosing as 0.01, 0.05 and 0.10, respectively; $\mathbf{N}_{\text{noise}}$ is white noise.

The identification results can be evaluated by relatively percentage error (RPE) values between the true force and the identified force as

$$\text{RPE} = \frac{\|\mathbf{f}_{\text{identified}} - \mathbf{f}_{\text{true}}\|}{\|\mathbf{f}_{\text{true}}\|} \times 100\% \tag{25}$$

where $\mathbf{f}_{\text{true}}$ is the true force and $\mathbf{f}_{\text{identified}}$ is the identified force. In addition, a novel optimal truncating point selection criterion is proposed in the paper, which can be expressed by minimizing the RPE values of MFI as follow

$$\text{RPE}_{k(opt)} = \min_{k\in(0,n]} \{\text{RPE}_k\} \tag{26}$$

If error level $E_p = 0.1$, the simulation of the bending moment and acceleration responses at 1/4 span of the simply supported beam are shown in Fig. 3. The illustration results show that bending moment responses are more likely to be disturbed by white noise than the acceleration responses due to the magnitude of bending moment responses in the high frequency range is very small compared with the magnitude of acceleration responses (Law et al., 2001). Due to the larger differences between the simulation responses and the true responses of bending moment responses, it is more difficult to identify the moving force from the bending moment responses and the identification accuracy should be relatively poor compared with acceleration responses.

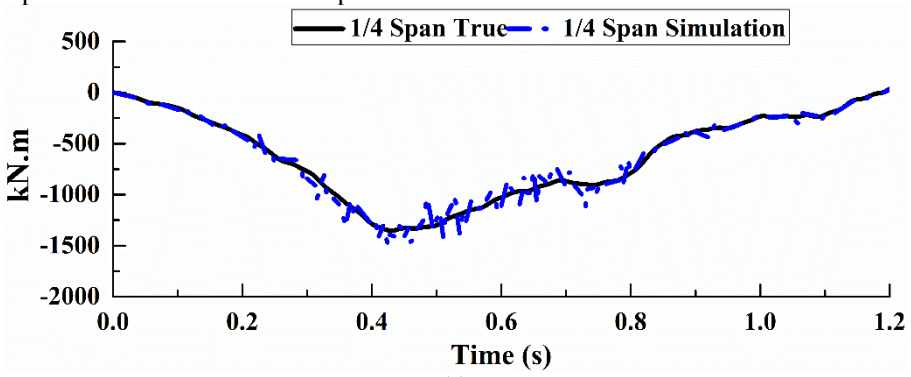

(a)

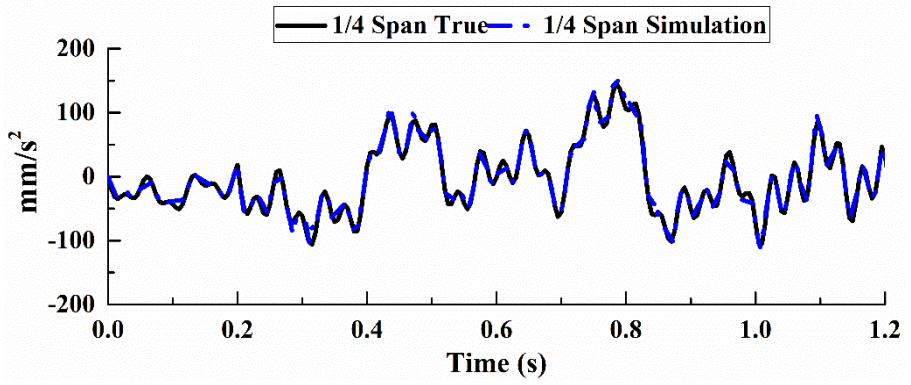

(b)

Fig. 3. The true responses and simulation responses at 1/4 span for moving force identification with 10% error level: (a) Bending moment responses; (b) Acceleration responses.

3.2 Choosing the optimal regularization matrix L for PP-TSVD

In this section, the regularization matrix $\mathbf{L}$ of the PP-TSVD will be chosen in MFI with different cases. As mentioned above, $\mathbf{L}$ is $\big(n-(p-1)\big)\times n$ and a band matrix, the p is corresponding to $(p-1)$-th derivative operator. Moreover, if $p=1$ such that $\mathbf{L}_1$ is the unity matrix, then the PP-TSVD is similar to TSVD in this case. If $p=2$ such that $\mathbf{L}_2$ approximates the first derivative operator, then the solution of PP-TSVD $\mathbf{x}_{\mathbf{L},k}$ represents a piecewise constant function with at most k discontinuities. If $p=3$ such that $\mathbf{L}_3$ approximates the second derivative operator, then $\mathbf{x}_{\mathbf{L},k}$ represents a continuous function consisting of at most $k-1$ straight lines. The $\mathbf{L}_4$ is approximations to the third derivative operator corresponding to $p=4$. The regularization matrices $\mathbf{L}_1$, $\mathbf{L}_2$, $\mathbf{L}_3$ and $\mathbf{L}_4$ are corresponding to TSVD, PP-TSVD ($\mathbf{L}_2$), PP-TSVD ($\mathbf{L}_3$) and PP-TSVD ($\mathbf{L}_4$), respectively, which can be shown as follows

$$
\mathbf{L}_1=\begin{pmatrix}1 & & & \\ & 1 & & \\ & & \ddots & \\ & & & 1\end{pmatrix}_{n\times n}
$$

$$
\mathbf{L}_2=\begin{pmatrix}-1 & 1 & & & \\ & -1 & 1 & & \\ & & \ddots & \ddots & \\ & & & -1 & 1\end{pmatrix}_{(n-1)\times n}
$$

$$
\mathbf{L}_3=\begin{pmatrix}1 & -2 & 1 & & \\ & 1 & -2 & 1 & \\ & & \ddots & \ddots & \ddots \\ & & & 1 & -2 & 1\end{pmatrix}_{(n-2)\times n} \tag{27}
$$

$$
\mathbf{L}_4=\begin{pmatrix}-1 & 3 & -3 & 1 & & \\ & -1 & 3 & -3 & 1 & \\ & & \ddots & \ddots & \ddots & \ddots \\ & & & -1 & 3 & -3 & 1\end{pmatrix}_{(n-3)\times n}
$$

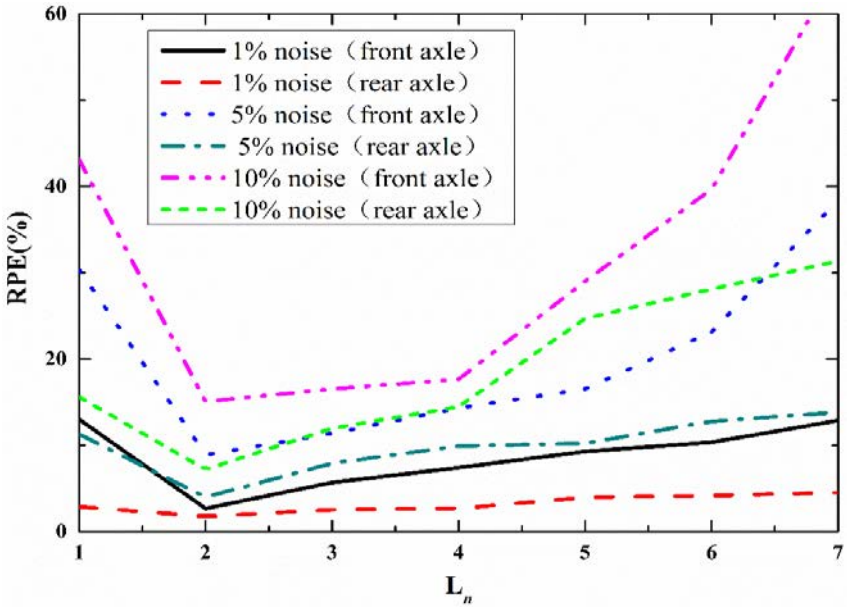

Fig. 4. MFI by PP-TSVD with different regularization matrices using responses at 1/4m, 1/4a and 1/2a

The RPE values of biaxial time-varying forces identified from combined responses (1/4m&1/4a&1/2a) by PP-TSVD with different regularization matrices are shown in Fig. 4. The illustration results show that the RPE values change little with regularization matrix $\mathbf{L}$ from the $\mathbf{L}_1$ to $\mathbf{L}_7$ when 1% noise level adopted. However, when larger noise levels such as 5% and 10% are used, the RPE values are increased significantly especially for higher-order derivative operators. The result indicates that the regularization matrix $\mathbf{L}_2$, i.e., the first derivative operator has much better noise

immunity than other derivative operators. We have simulated this problem with different moving force identification examples and found that the regularization matrix $\mathbf{L}_2$ of PP-TSVD is always the optimal which can be used in real applications directly.

Table 1

Comparison on RPE(%) values identified by TDM(SVD), TSVD and PP-TSVD with two kinds of regularization matrices

Sensors location	regularization matrix**L**	1% noise		5% noise		10% noise		20% noise	
		front axle	rear axle	front axle	rear axle	front axle	rear axle	front axle	rear axle
1/4m&1/2m&3/4m	TDM(SVD)	98.0	56.6	*	*	*	*	*	*
	TSVD	(65.2)	(35.2)	(*)	(86.3)	(*)	(*)	(*)	(*)
	PP-TSVD($\mathbf{L}_2$)	6.0	5.1	18.8	11.1	19.6	17.0	24.1	21.5
	PP-TSVD($\mathbf{L}_3$)	*9.5*	*5.5*	*22.3*	*11.4*	*29.4*	*17.1*	*40.8*	*28.0*
1/4a&1/2a	TDM(SVD)	9.0	2.7	45.2	13.6	90.4	27.3	*	54.6
	TSVD	(8.1)	(2.5)	(28.5)	(12.0)	(43.3)	(13.2)	(42.5)	(26.7)
	PP-TSVD($\mathbf{L}_2$)	2.9	1.0	7.9	5.6	14.7	6.3	23.8	11.2
	PP-TSVD($\mathbf{L}_3$)	*7.7*	*1.2*	*16.8*	*6.4*	*23.3*	*8.7*	*39.3*	*9.7*
1/4a&1/2a&3/4a	TDM(SVD)	0.6	0.3	2.5	1.4	5.1	2.8	10.2	5.5
	TSVD	(0.6)	(0.3)	(2.5)	(1.4)	(5.1)	(2.8)	(10.2)	(5.5)
	PP-TSVD($\mathbf{L}_2$)	0.6	0.3	2.5	1.4	5.1	2.8	10.2	5.5
	PP-TSVD($\mathbf{L}_3$)	*0.6*	*0.3*	*2.5*	*1.4*	*5.1*	*2.8*	*10.2*	*5.5*
1/2m&1/2a	TDM(SVD)	*	58.4	*	*	*	*	*	*
	TSVD	(83.0)	(36.4)	(*)	(62.9)	(*)	(63.0)	(*)	(65.6)
	PP-TSVD($\mathbf{L}_2$)	6.5	4.5	14.1	8.8	19.3	10.9	32.0	11.6
	PP-TSVD($\mathbf{L}_3$)	*8.6*	*8.9*	*14.7*	*14.4*	*29.2*	*14.6*	*49.1*	*19.5*
1/4m&1/2m&1/2a	TDM(SVD)	*	30.7	*	*	*	*	*	*
	TSVD	(72.3)	(25.1)	(92.5)	(59.8)	(92.0)	(63.2)	(99.9)	(69.7)
	PP-TSVD($\mathbf{L}_2$)	5.2	2.1	10.3	8.3	16.9	11.1	32.6	14.2
	PP-TSVD($\mathbf{L}_3$)	*5.3*	*6.8*	*12.6*	*10.7*	*22.9*	*12.8*	*43.9*	*18.5*
1/4m&1/2m&1/4a&1/2a	TDM(SVD)	10.1	3.6	50.3	18.0	*	36.0	*	72.1
	TSVD	(9.7)	(3.0)	(26.3)	(11.6)	(42.3)	(18.0)	(46.7)	(28.3)
	PP-TSVD($\mathbf{L}_2$)	2.4	1.3	8.8	3.3	13.5	6.1	25.8	11.8
	PP-TSVD($\mathbf{L}_3$)	*8.0*	*1.3*	*11.5*	*3.9*	*19.5*	*6.8*	*35.7*	*13.1*
1/4m&1/4a&1/2a	TDM(SVD)	9.7	2.3	40.5	10.9	96.9	21.8	*	43.5
	TSVD	(9.0)	(1.9)	(30.4)	(10.3)	(43.1)	(15.6)	(41.9)	(29.7)
	PP-TSVD($\mathbf{L}_2$)	2.6	1.7	8.9	4.0	15.1	7.2	25.5	12.3
	PP-TSVD($\mathbf{L}_3$)	*7.4*	*1.8*	*12.1*	*4.5*	*19.4*	*8.4*	*32.1*	*12.7*
1/2m&1/4a&1/2a	TDM(SVD)	9.8	3.3	48.8	16.7	97.6	33.5	*	67.2
	TSVD	(9.6)	(2.8)	(26.9)	(11.1)	(45.1)	(13.2)	(47.3)	(26.9)
	PP-TSVD($\mathbf{L}_2$)	2.7	1.3	9.5	2.3	16.3	5.7	25.1	10.8
	PP-TSVD($\mathbf{L}_3$)	*5.5*	*1.5*	*13.4*	*2.5*	*21.5*	*6.6*	*33.9*	*38.3*

TDM: time domain method; SVD: singular value decomposition; TSVD: truncated singular value decomposition; PP-TSVD: piecewise polynomial truncated singular value decomposition.

1/4, 1/2, and 3/4 represent the measurement location at a quarter, middle span, and three quarters, respectively. The letters ‘‘m’’ and ‘‘a’’ represent the bending moment and acceleration responses, respectively. Underlined RPE(%) values are for PP-TSVD with double diagonal matrix $\mathbf{L}_2$, italics RPE(%) values are for PP-TSVD with tri-diagonal matrix $\mathbf{L}_3$, RPE(%) values in parentheses are for TSVD with unity matrix $\mathbf{L}_1$, and other values are for conventional counterpart SVD embedded in TDM. The symbol ‘‘*’’ represents that the RPE(%) value is bigger than 100%.

There are 8 cases in Table 1 for evaluating the identification accuracy of TDM(SVD), TSVD and PP-TSVD with two kinds of regularization matrices. The identification results of rear axle force are better than front axle force in all cases due to the weight of the front axle is less than half of the rear axle. Due to the bridge weight remains the same, the heavier the axle is, the greater the mass ratio of axle-bridge will be, and then the greater the dynamic responses will be. The identification accuracy is improved with the increase of the mass ratio of axle-bridge or the increase of the dynamic responses.

As shown in Table 1, most of the RPE(%) values of TDM(SVD) are bigger than 90% when white noise level reaches 10%. The identification accuracy of TSVD has obvious improved compared with TDM(SVD). Moreover, the RPE values of PP-TSVD have significant improvement compared with TSVD in most of the cases, which indicate that

the PP-TSVD has excellent theoretical completeness and the ability to offset the disadvantage of TSVD perfectly by extracting the true responses from truncated small singular values and superposes it into the solution of TSVD.

When noise level reaches 20%, the PP-TSVD with regularization matrix $\mathbf{L}_3$ has quite precise identification results and the biggest RPE value is less than 50% in all cases, which has higher identification accuracy and stronger robustness compared with TSVD. Moreover, the PP-TSVD with regularization matrix $\mathbf{L}_2$ has very precise identification results and the biggest RPE value is less than 35% in all cases with 20% noise level, which has much better identification results compared with PP-TSVD($\mathbf{L}_3$). The results show that the regularization matrix is very important to the PP-TSVD, which affects the identification accuracy and robustness of the PP-TSVD in MFI.

The identified front axle force and rear axle force with different responses and noise levels are shown in Fig. 5 to Fig. 10. Illustration results show that the identified forces and PSD curves agree well with the true forces in all cases except for the case of TSVD which has significant deviation when bending moment responses used alone. In this case, quite a lot of small singular values have been truncated by TSVD method and then the over-fitting problem is revealed. By choosing the optimal regularization matrix $\mathbf{L}_2$, the PP-TSVD has better adaptability with sensors location as shown in the forces identification results and PSD curves from Fig. 5 to Fig. 10, which also has better noise immunity and robust with ill-posed problems. Finally, the optimal regularization matrix for the PP-TSVD is $\mathbf{L}_2$ and it will be adopted in the following studies. In this section, the best truncating point k of the PP-TSVD algorithm is default used in all cases and the selection of the optimal truncating point k of the PP-TSVD will be studied in the next section.

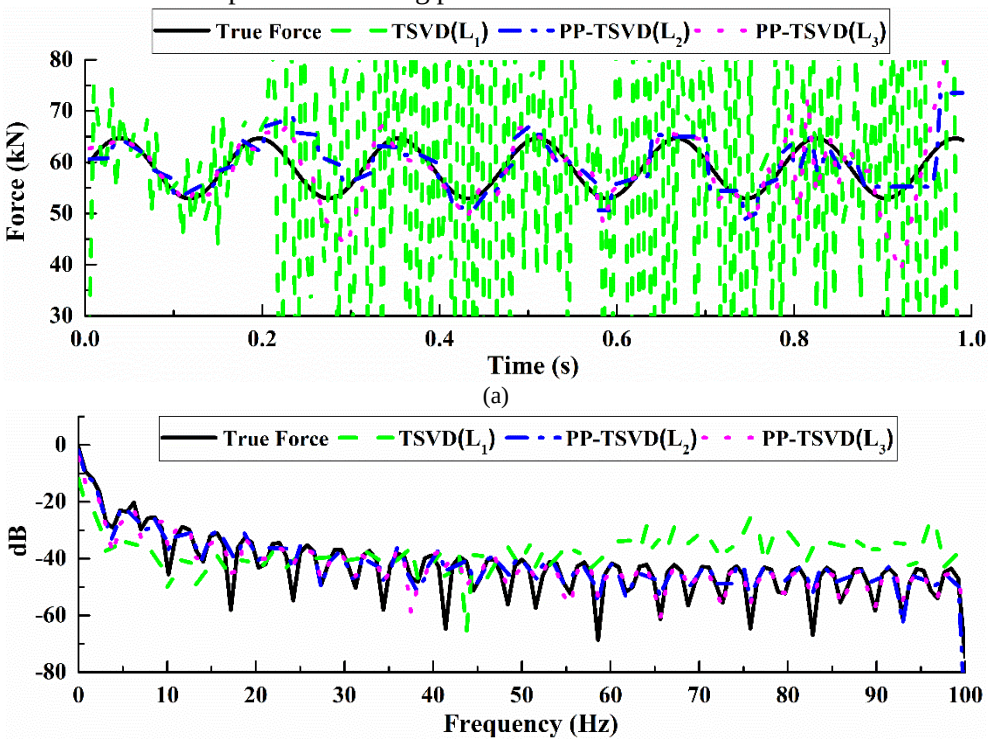

Fig. 5. The identified front axle force from bending moment responses by TSVD and PP-TSVD with two kinds of regularization matrices (1/4m&1/2m&3/4m 1% Noise): (a) The front axle force; (b) The PSD of the front axle.

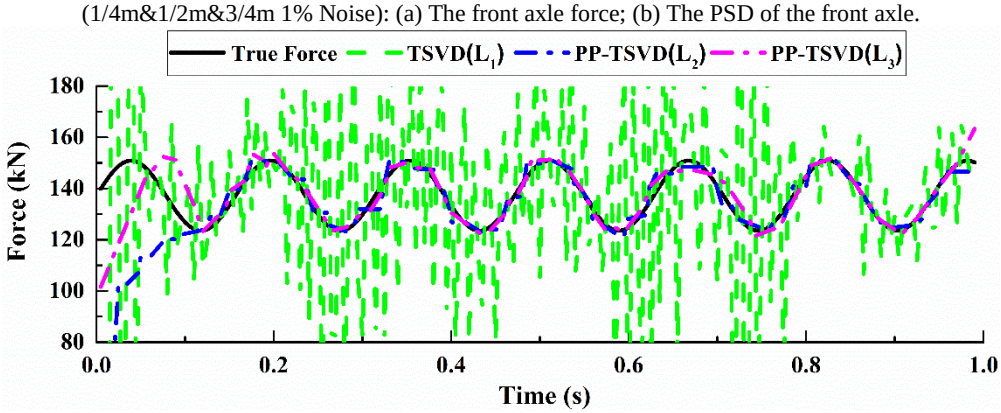

(a)

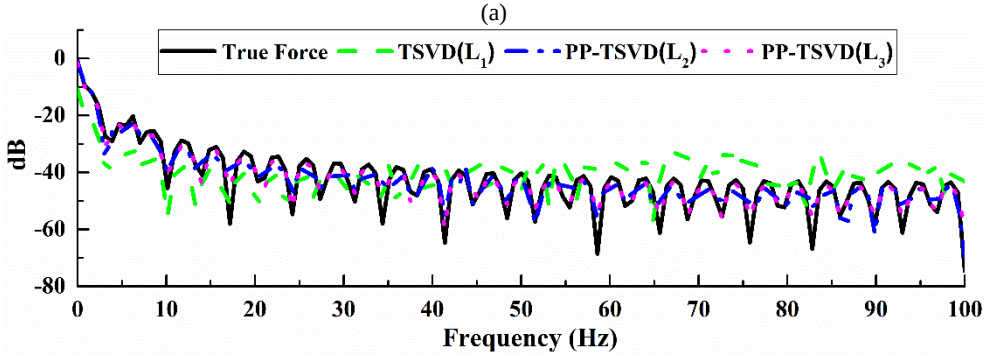

(b)

Fig. 6. The identified rear axle force from bending moment responses by TSVD and PP-TSVD with two kinds of regularization matrices (1/4m&1/2m&3/4m 1% Noise): (a) The rear axle force; (b) The PSD of the rear axle.

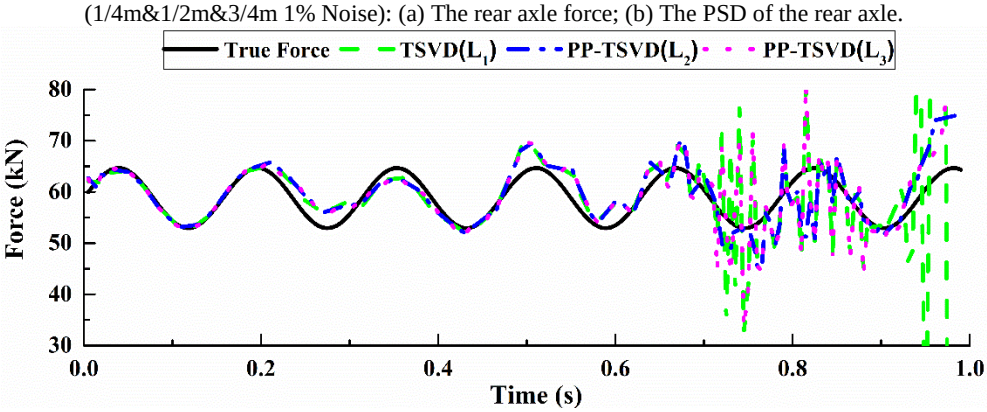

(a)

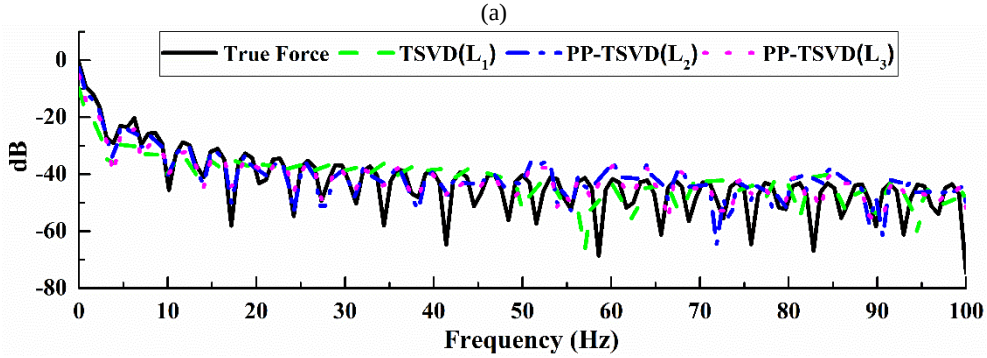

(b)

Fig. 7. The identified front axle force from combined responses by TSVD and PP-TSVD with two kinds of regularization matrices (1/4m&1/4a&1/2a 5% Noise): (a) The front axle force; (b) The PSD of the front axle.

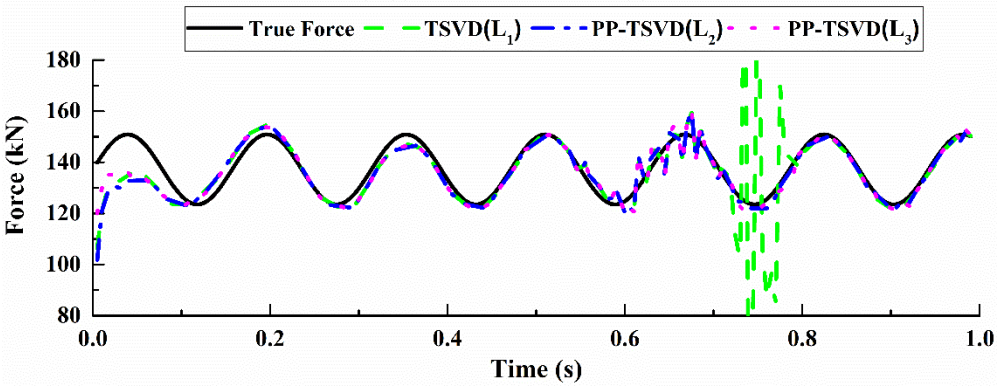

(a)

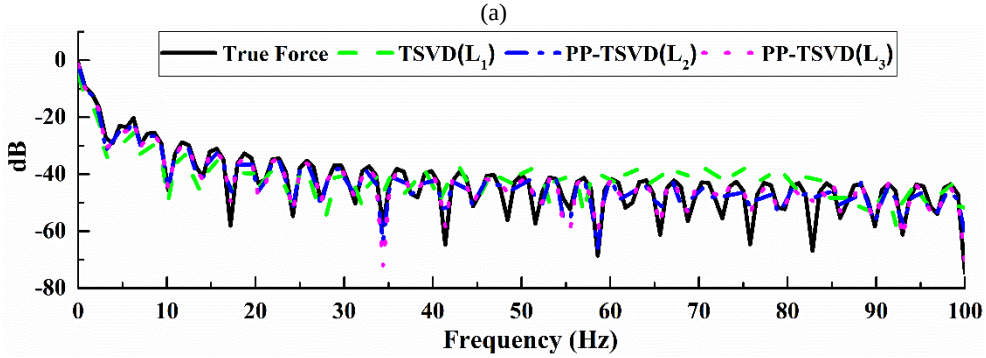

(b)

Fig. 8. The identified rear axle force from combined responses by TSVD and PP-TSVD with two kinds of regularization matrices (1/4m&1/4a&1/2a 5% Noise): (a) The rear axle force; (b) The PSD of the rear axle.

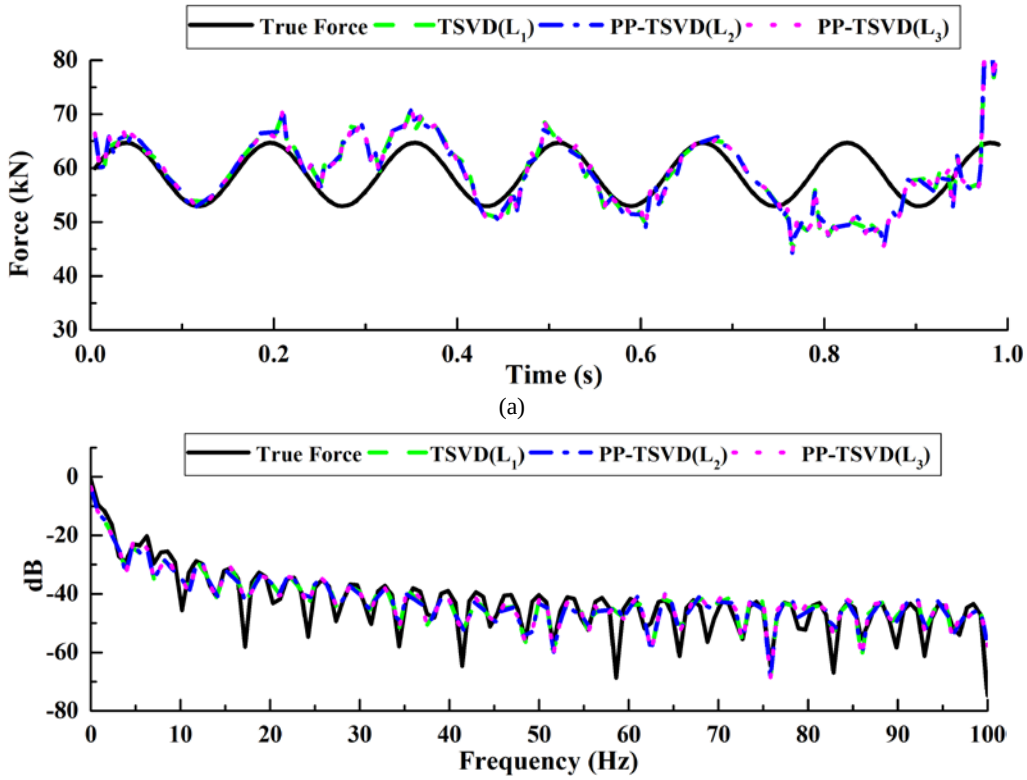

(a)

(b)

Fig. 9. The identified front axle force from acceleration responses by TSVD and PP-TSVD with two kinds of regularization matrices (1/4a&1/2a&3/4a 20% Noise): (a) The front axle force; (b) The PSD of the front axle.

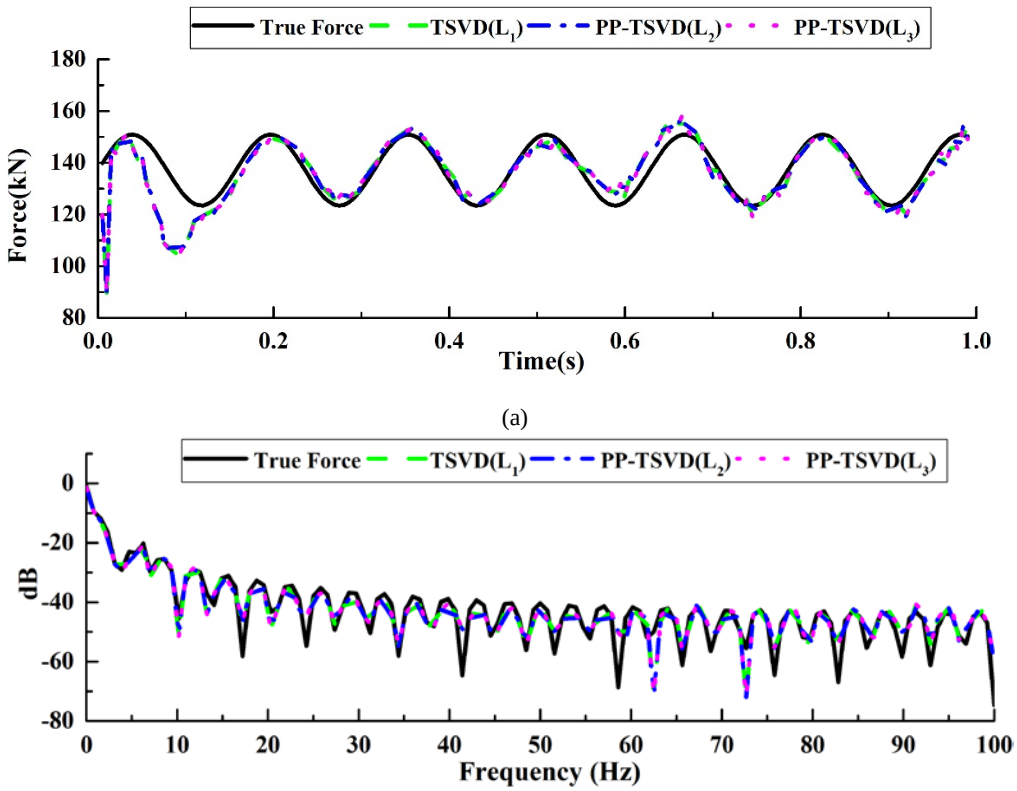

(a)

(b)

Fig. 10. The identified rear axle force from acceleration responses by TSVD and PP-TSVD with two kinds of regularization matrices (1/4a&1/2a&3/4a 20% Noise): (a) The rear axle force; (b) The PSD of the rear axle.

3.3 Choosing the optimal truncating point k of PP-TSVD

The truncating point k controls the amount of stabilization imposed on $\mathbf{x}_k$ and the calculation accuracy of TSVD. Obviously, the bigger the truncating point k is, the more information from the right-hand side is actually used. Here,

the total number of samples n is 396 and $n = 396 \geq k \geq 1$. Especially, when $k = n$ is adopted, no small singular values are truncated and then the TDM, TSVD, and PP-TSVD show same results. However, when the small singular values are truncated, there are also some useful responses neglected containing in the small singular values from the right-hand side **b**. PP-TSVD can overcome this problem of TSVD by extracting the true responses from truncated small singular values and superposes it into the solution of TSVD.

Table 2
The optimal truncating point *k* of PP-TSVD($\mathbf{L}_2$) with three kinds of noise level

Case	Sensors location	1% noise	5% noise	10% noise
1	1/4m&1/2m&3/4m	127	108	94
2	1/4a&1/2a	387	375	374
3	1/4a&1/2a&3/4a	396	396	396
4	1/2m&1/2a	261	246	246
5	1/4m&1/2m&1/2a	285	262	262
6	1/4m&1/2m&1/4a&1/2a	375	382	365
7	1/4m&1/4a&1/2a	387	382	375
8	1/2m&1/4a&1/2a	387	379	374

Table 2 tabulates the optimal truncating point *k* of the PP-TSVD with three random noise levels in all 8 cases, which shows the higher the noise level is, the smaller truncating point should be chosen. That is, the greater the responses are contaminated by measurement errors, the more small singular values need to be truncated.

In addition, the higher the acceleration responses ratio is in the combined responses, the bigger truncating point should be chosen, which indicates that the noise has less impact on acceleration responses due to their high frequency characteristic, and then there will be less small singular values contained in matrix **A**. Especially, when MFI from acceleration responses alone as case 3, the truncating point $k = 396$ is the total number of samples n as shown in Fig. 11, which indicates that the matrix **A** equals to the matrix $\mathbf{A_k}$. That is, no small singular values are truncated and no additional responses are extracted from truncated small singular values. In this case, the identification results and the PSD curves by TSVD and PP-TSVD are the same, as shown in Table 1 and Fig. 9 to Fig. 10.

In contrast, the higher the bending moment responses ratio is in the combined responses, the smaller truncating point should be chosen, which indicates that the noise has more impact on bending moment responses due to their low frequency characteristic, and then more small singular values need to be truncated. In this case, it is obviously necessary to extract the true responses from truncated small singular values by the PP-TSVD, and then the identification results and the RPE values are much improved compared with the TSVD as modification value $-\mathbf{V}_k\mathbf{w}_k$.

As shown in Fig. 12, when acceleration responses used alone in MFI, most of measured responses are useful and the number of the small values is very small. However, if the truncating point *k* is taken at 396 the RPE values will be increased sharply due to very ill-posed matrix of **A** which is caused by small singular values. Therefore, it is obviously important to truncate very small singular values of matrix **A**, even if the number is very small.

As shown in Fig. 13, when bending moment and acceleration responses are both used in the combined responses, RPE values are increased dramatically when the truncating point *k* is greater than 250. Moreover, there is a typical crest when the truncating point near 100, which also should be avoided to maintain reasonable RPE values of MFI.

As shown in Fig. 14, when bending moment responses used alone in MFI, RPE values are increased dramatically when the truncating point *k* is bigger than 100. In this case, the optimal truncating point *k* is very small and then there are many small singular values that need to be truncated. Therefore, the identification results of PP-TSVD are much improved than TSVD by extracting the true responses and superposing it into the solution of TSVD as in Table 1 and Fig. 5 to Fig. 6.

In summary, the type of sensors has great influence on the selection of the optimal truncation parameter k. Moreover, the position of truncating point has great effect on the performance of PP-TSVD in comparison with TSVD:

if the truncating point k is small, there are many useful responses that can be extracted from truncated small singular values and then the identification accuracy of PP-TSVD is superior than that of TSVD. On the contrary, if the truncating point k is large and close to the total number of samples n, there would be only few useful responses to be extracted and the improvement made by PP-TSVD becomes modest compared with TSVD.

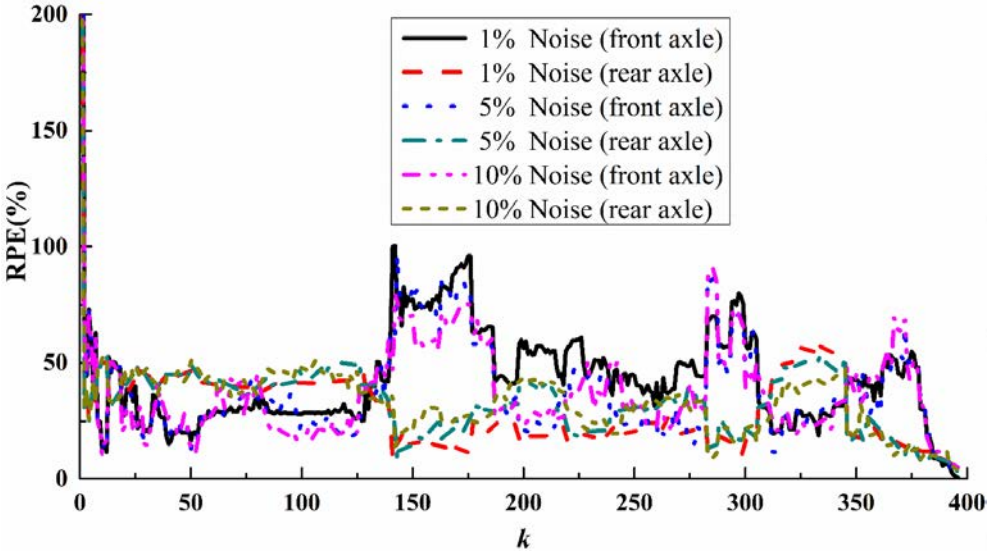

Fig. 11. Influence of truncating point k of PP-TSVD on MFI from acceleration responses (1/4a&1/2a&3/4a)

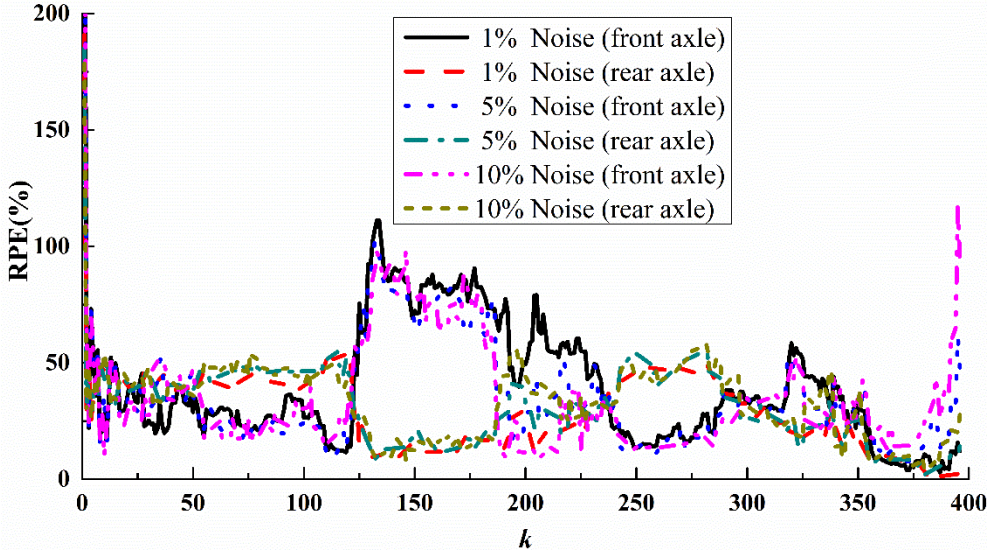

Fig. 12. Influence of truncating point k of PP-TSVD on MFI from acceleration responses (1/4a&1/2a)

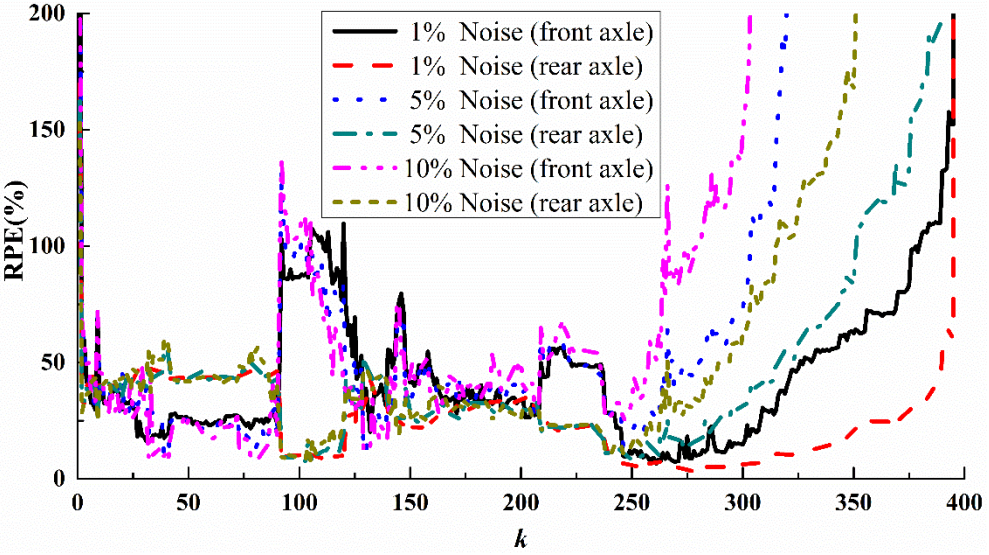

Fig. 13. Influence of truncating point k of PP-TSVD on MFI from combined responses (1/2m&1/2a)

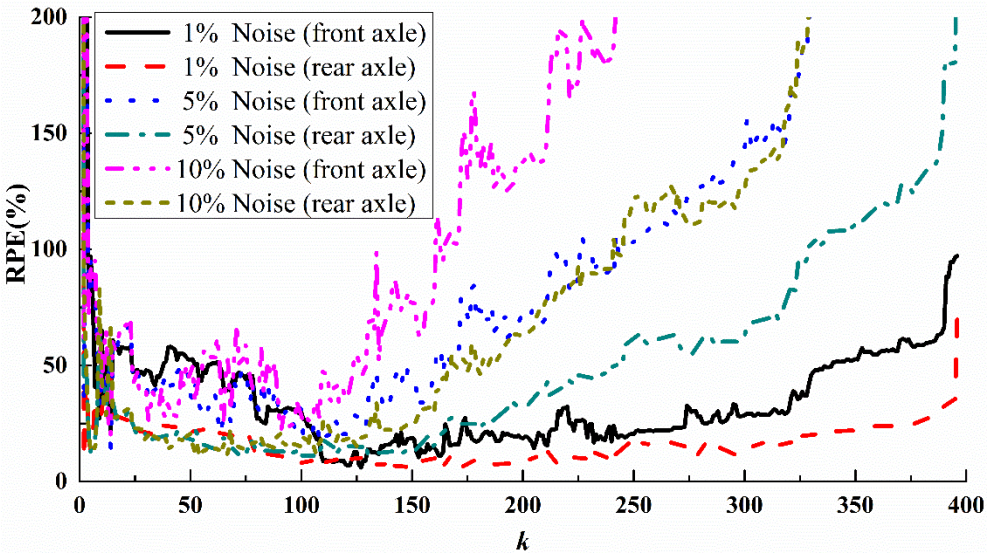

Fig. 14. Influence of truncating point *k* of PP-TSVD on MFI from bending moment responses (1/4m&1/2m&3/4m)

4 Conclusions

In this work, a novel algorithm called PP-TSVD was introduced in MFI and a comparative study was made to evaluate this technique against TSVD and the SVD embedded in the TDM. By means of numerical simulations, a comprehensive parametric study has been done and the following conclusions can be drawn:

By truncating small singular values to improve the condition of matrix **A**, the TSVD can partially solve the ill-posed problem occurred with the SVD-based methods such as TDM due to the impact of small singular values. Even though TSVD can cope reasonably well with the ill-posed problem in MFI process, its accuracy is still not very good as this technique ignores all the $n-k$ small singular values which contain some useful responses. The PP-TSVD can not only solve ill-posed problem as TSVD, but also extracts the true responses and superposes it into the solution of TSVD as a modification value, which has excellent theoretical completeness and offset the disadvantage of TSVD perfectly.

By choosing the optimal regularization matrix, the PP-TSVD has better adaptability with different type of responses (acceleration, bending moment or their combination) and number of sensors. This technique also has better noise immunity and robust with ill-posed problems. The first derivative operator $\mathbf{L}_2$ has much better noise immunity than other derivative operators, which will serve as the optimal regularization matrix for the PP-TSVD.

Finally, it is found that the identification accuracy and ill-posed immunity of the PP-TSVD is also influenced by the truncating point k, which shows that for the higher of the noise level, the smaller truncating point should be chosen to enhance the accuracy of the technique. When the optimal truncating point k is 396 which equals to the total number of samples n in this special case 3, no small singular values are truncated and then the ill-posed immunity of PP-TSVD can not be reflected. In this case, all methods showed same results regardless of the type of methods such as TDM, TSVD, and PP-TSVD. In practical implementation of MFI, there must be some small singular values that need to be truncated because the total number of samples will be a much larger number compared with the simple numerical simulation. In this circumstance, PP-TSVD will be superior to other methods. Acceleration responses or combination responses were shown to facilitate more accurate MFI by PP-TSVD hence they are highly recommended as the main response data for use with the PP-TSVD based MFI procedure. Due to their low frequency characteristic and possible impact by measurement noise, the use of bending moment responses alone is not recommended.

Acknowledgments

This work is supported by the Key Science and Technology Program of Henan Province, China (192102310011), the Science and Technology Innovation Team of Eco-building Material and Structural Engineering in the University of Henan Province, China (13IRTSTHN002), and the University-industry Collaboration Project of Henan Province, China (142107000088).

References:

Bouhamidi A, Jbilou K, Reichel L, et al. (2011) An extrapolated TSVD method for linear discrete ill-posed problems with Kronecker structure. *Linear Algebra and Its Applications* 434(7): 1677-1688.

Busby HR and Trujillo DM (1997) Optimal regularization of an inverse dynamics problem. *Computers & structures* 63(2): 243-248.

Chan THT and Ashebo DB (2006) Theoretical study of moving force identification on continuous bridges. *Journal of sound and Vibration* 295(3-5): 870-883.

Chan THT, Law SS, Yung TH, et al. (1999) An interpretive method for moving force identification. *Journal of sound and vibration* 219(3): 503-524.

Chan THT, Yu L, Law SS, et al. (2001) Moving force identification studies, I: theory. *Journal of Sound and Vibration* 247(1): 59-76.

Chen Z and Chan THT (2017) A truncated generalized singular value decomposition algorithm for moving force identification with ill-posed problems. *Journal of Sound and Vibration* 401: 297-310.

Chen Z, Chan THT and Nguyen A (2018) Moving force identification based on modified preconditioned conjugate gradient method. *Journal of Sound and Vibration* 423: 100-117.

Choi HG, Thite AN and Thompson DJ (2007) Comparison of methods for parameter selection in Tikhonov regularization with application to inverse force determination. *Journal of Sound and Vibration* 304(3-5): 894-917.

Ding Y, Zhao BY, Wu B, et al. (2015) Simultaneous identification of structural parameter and external excitation with an improved unscented Kalman filter. *Advances in Structural Engineering* 18(11): 1981-1998.

Dowling J, OBrien EJ and González A (2012) Adaptation of Cross Entropy optimisation to a dynamic Bridge WIM calibration problem. *Engineering Structures* 44: 13-22.

Feng DM, Sun H and Feng MQ (2015) Simultaneous identification of bridge structural parameters and vehicle loads. *Computers & Structures* 157: 76-88.

Giustolisi O (2004) Sparse solution in training artificial neural networks. *Neurocomputing* 56: 285-304.

Hansen PC and Mosegaard K (1996) Piecewise polynomial solutions without a priori break points. *Numerical linear algebra with applications* 3(6): 513-524.

Law SS, Chan THT and Zeng QH (1999) Moving force identification-a frequency and time domains analysis. *Journal of dynamic systems, measurement and control* 121(3): 394-401.

Law SS, Chan THT and Zeng QH (1997) Moving force identification: a time domain method. *Journal of Sound and vibration* 201(1): 1-22.

Law SS, Chan THT, Zhu QX, et al. (2001) Regularization in moving force identification. *Journal of Engineering Mechanics* 127(2): 136-148.

Li J, Law SS and Hao H (2013) Improved damage identification in bridge structures subject to moving loads: numerical and experimental studies. *International Journal of Mechanical Sciences* 74: 99-111.

Liu J, Meng XH, Zhang DQ, Jiang C, et al. (2017) An efficient method to reduce ill-posedness for structural dynamic load identification. *Mechanical Systems and Signal Processing* 95: 273-285.

Liu J, Sun XS, Han X, et al. (2015) Dynamic load identification for stochastic structures based on Gegenbauer polynomial approximation and regularization method. *Mechanical Systems and Signal Processing* 56: 35-54.

Lu ZR and Liu JK (2011) Identification of both structural damages in bridge deck and vehicular parameters using measured dynamic responses. *Computers & Structures* 89(13-14): 1397-1405.

O'Connor C and Chan THT (1988) Dynamic wheel loads from bridge strains. *Journal of Structural Engineering* 114(8): 1703-1723.

Pan CD, Yu L, Liu HL, et al. (2018) Moving force identification based on redundant concatenated dictionary and weighted l_1-norm regularization. *Mechanical Systems and Signal Processing* 98: 32-49.

Pinkaew T (2006) Identification of vehicle axle loads from bridge responses using updated static component technique. *Engineering Structures* 28(11): 1599-1608.

Ronasi H, Johansson H and Larsson F (2011) A numerical framework for load identification and regularization with application to rolling disc problem. *Computers & structures* 89(1-2): 38-47.

Sanchez J and Benaroya H (2014) Review of force reconstruction techniques. *Journal of Sound and Vibration* 333(14): 2999-3018.

Sobouti A, Motagh M and Sharifi MA (2016) Inversion of surface gravity data for 3-D density modeling of geologic structures using total variation regularization. *Studia Geophysica et Geodaetica* 60(1): 69-90.

Winkler JR (1997a) Polynomial basis conversion made stable by truncated singular value decomposition. *Applied Mathematical Modelling* 21(9): 557-568.

Winkler JR (1997b) Tikhonov regularisation in standard form for polynomial basis conversion. *Applied Mathematical Modelling* 21(10): 651-662.

Xu PL (1998) Truncated SVD methods for discrete linear ill-posed problems. *Geophysical Journal International* 135(2): 505-514.

Yu L and Chan THT (2007) Recent research on identification of moving loads on bridges. *Journal of Sound and Vibration* 305(1-2): 3-21.

Yu L, Chan THT and Zhu JH (2008) A MOM-based algorithm for moving force identification: Part II-Experiment and comparative studies. *Structural Engineering and Mechanics* 29(2): 155-169.

Yu Y, Cai CS and Deng L (2016) State-of-the-art review on bridge weigh-in-motion technology. *Advances in Structural Engineering* 19(9): 1514-1530.

Zhu XQ and Law SS (2006) Moving load identification on multi-span continuous bridges with elastic bearings. *Mechanical Systems and Signal Processing* 20(7): 1759-1782.

Zhu XQ, Law SS, Huang L, et al. (2018) Damage identification of supporting structures with a moving sensory system. *Journal of Sound and Vibration* 415: 111-127.